Quantifying epistemic uncertainty in volcanology using structured expert judgment methods

Application to the Campi Flegrei caldera (Italy)

Andrea Bevilacqua, Willy Aspinall, Augusto Neri
Istituto Nazionale di Geofisica e Vulcanologia, Sezione di Pisa

Uncertainty in Geoscience: a workshop on hazard analysis.
University at Buffalo (SUNY), 15-17th March 2016

The volcano can be assumed as a **random system** that must be assessed with incomplete and **uncertain information**.

The **forecast** of its behavior cannot be easily constrained by using simple probability models.

Adopting a **doubly stochastic approach,** the ill-constrained parameters of the probability models are themselves represented as additional random variables.

Uncertainty quantification assumes a great importance, and we distinguished:

I. the **physical variability,** i.e. the intrinsic randomness of the system under study,
II. the **epistemic uncertainty** due to the imperfect knowledge of the system.

As a consequence of this approach, all the probability estimates have their own confidence intervals.

Example: assume to roll an unknown dice, which could have 6 or 20 faces with equal chances.

The probability P of the event of getting a number N > 3 is 50% in the first case, but it is 85% in the second.

Following a doubly stochastic approach, we might say that
P is 67.5% in mean, with an uncertainty range from 50% to 85%.

Even the probability maps will be affected by uncertainty: for this reason we calculated the **mean, 5th and 95th percentile** values for all the probability density functions and volcanic hazard estimates.

Expert judgement methods

In general, when forward models or statistical procedures are not available, the quantification of epistemic uncertainty must be based directly on the **expert opinion**
(e.g. Cooke 1991, Aspinall 2006, 2010, Flandoli et al. 2011).

Expert judgement techniques are aimed at producing robust quantitative estimates relying on the views of a pool of experts, concerning:

- degrees of belief of alternative **conceptual models**
or
- unknown/uncertain **material quantities.**

Performance based elicitation procedures include an empirical step of expert ranking, aimed at measuring uncertainty quantification capabilities.

The EXCALIBUR software (http://www.expertsin-uncertainty.net/) is an available tool ready for use to assess such performance weights following the so called 'Classical method'.

Alternative subroutines are easy to produce with R statistics or similar software (i.e. MATLAB, Octave).

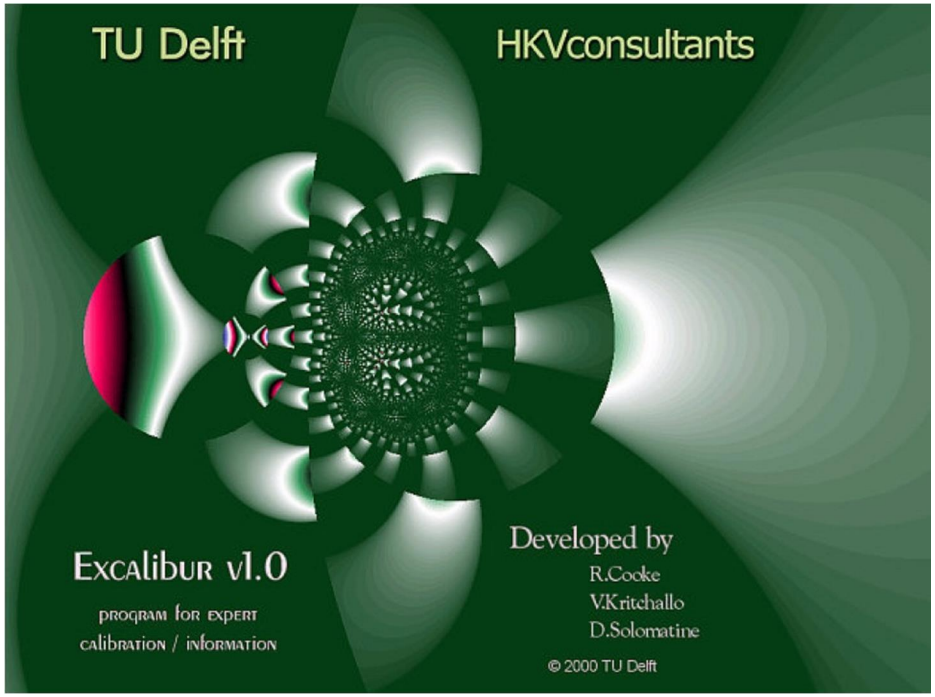

Fig 11. Opening screen of the EXCALIBUR software.

In general two informed questionnaires about numerical quantities are prepared:

- **The seed (or calibration) questions,** with known answers.
- **The target questions (or questions of interest)**.

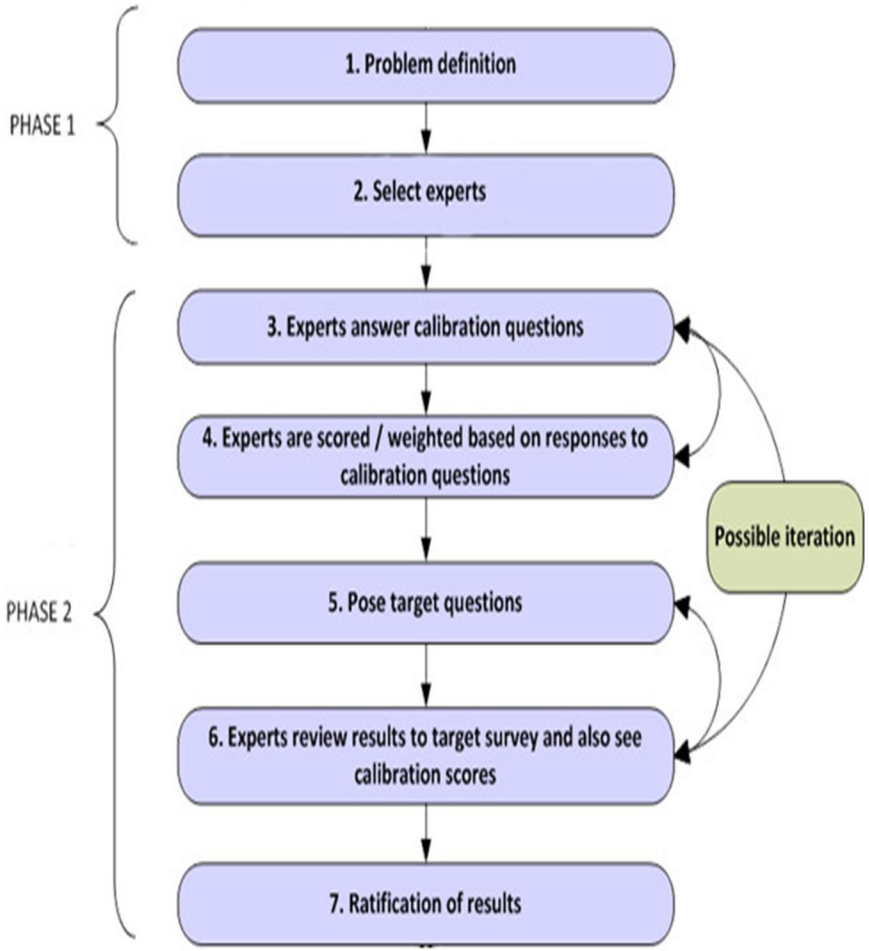

Fig 12. Phases of a structured elicitation session (courtesy of W. Aspinall).

For each question (seed or target), the experts express their views as the values of **the 5th, 50th and 95th percentiles** of a 'primitive' probability measure representing their uncertainty.

The seed questions concern known facts which must be inherent as much as possible with the scientific field of the target questions.

Indeed the answers to the seed questions are adopted for **scoring the experts'** uncertainty estimation performances.

The diverse answers to the **target questions** are then pooled using the obtained scores, and their combination defines a new virtual expert: the **global Decision Maker (DM)**.

Alternative performance based methods adopt different **performance scores, 'primitive' distributions and pooling rules** for combining the responses.

For the following application we computed three different **DM** using three different methods with different approaches:

• the **Cooke Classical Model (CM)**

• the **Expected Relative Frequency model (ERF)**

•an **Equal Weights pooling (EW)** of the experts' uncertainty densities

Expert / EJ method	***Expert 1***	***Expert 2***	***Expert 3***	***Expert 4***	***Expert 5***	***Expert 6***	***Expert 7***	***Expert 8***
Classical Method	3.2%	0.0%	0.0%	0.0%	6.8%	0.0%	89.9%	0.1%
Expected Relative Frequency	11.9%	7.8%	7.3%	8.8%	19.4%	13.4%	20.9%	10.5%
Equal weights	12.5%	12.5%	12.5%	12.5%	12.5%	12.5%	12.5%	12.5%

Tab 1. Example performance scoring percentages assuming the different scoring rules.

The Cooke classical method uses maximal entropy probability measures, uniform in each inter-quantile range.

The performance score is the product of two values:

Calibration score: likelihood that the true results correspond to the expert distributions.
It could be considered as a statistical accuracy.

Information score: average relative information w.r.t. a uniform distribution.
It penalizes too large uncertainty ranges.

The ERF method uses triangular distributions, with the 50th percentile used as the vertex of the triangle.

The performance score adopted is:

Expected relative frequency: expectation of the frequency of random answers which fall in a selected interval around true values.
It could be assumed as a point-wise accuracy.

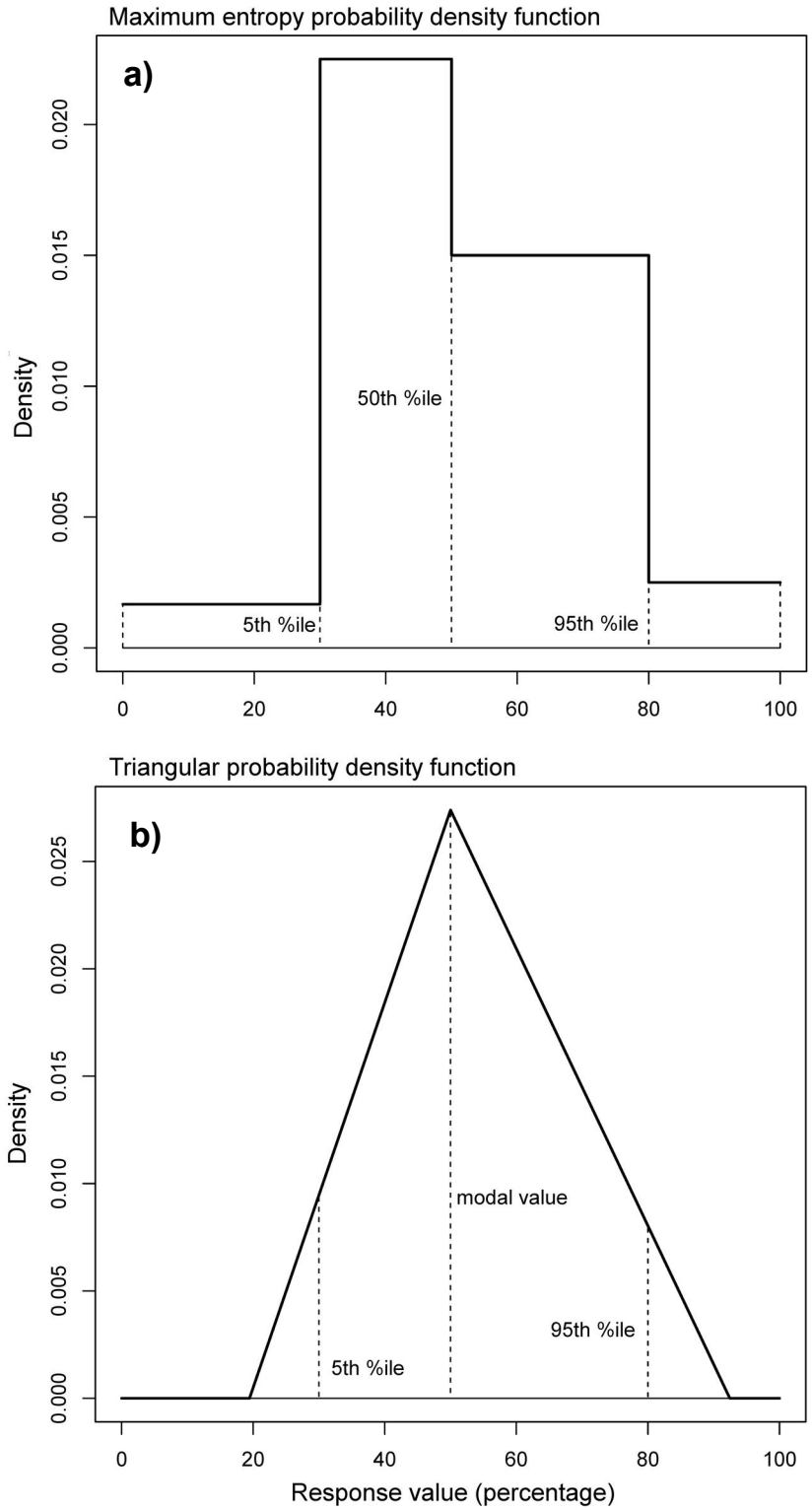

Fig 13. Examples of 'primitive' probability distributions for an expert response equal to [30% - 50 % - 80%].

Application to the Campi Flegrei caldera (Italy)

Campi Flegrei is an active volcanic area in the Campanian Plain, dominated by a 12 km large caldera.

A few hundreds of thousand people live inside the caldera, and more than **1 million people** live in the nearby city of Naples.

The study concerns Campi Flegrei **long-term hazard assessments**, primarily based on past eruption data and on the structural features of the volcanic system.

They are required for **land use and evacuation planning**, but constitute also the necessary background for short-term hazard assessments.

Estimating the **probability of the next eruption event, its size, location, time and type** is a very difficult issue because of

- the lack of detailed information on the deeper portions of the system
- the high complexity of the physical processes controlling it.

Fig 2. Mosaic of orthophotos of Campi Flegrei caldera and surrounding areas

• Campi Flegrei caldera was created by **two ancient huge eruptions:** Campanian Ignimbrite (CI - 40 ka BP) and Neapolitan Yellow Tuff (NYT - 15 ka BP);

• In the last 15 ka the **eruption vents were sparse** in the caldera and most of the eruptions were explosive;

• There were **3 eruptive epochs** of volcanic activity, alternated to long periods of quiescence.

	Start	Duration
Epoch I	[15 ka BP	~4.5 ka]
Epoch II	[9.6 ka BP	~0.5 ka]
Epoch III	[5.5 ka BP	~2 ka]

•The most recent 'Monte Nuovo' eruption was in AD 1538, after ~3-3.5 ka of quiescience.

• Now there is much hydrothermal activity and the caldera is in an **unrest state**.

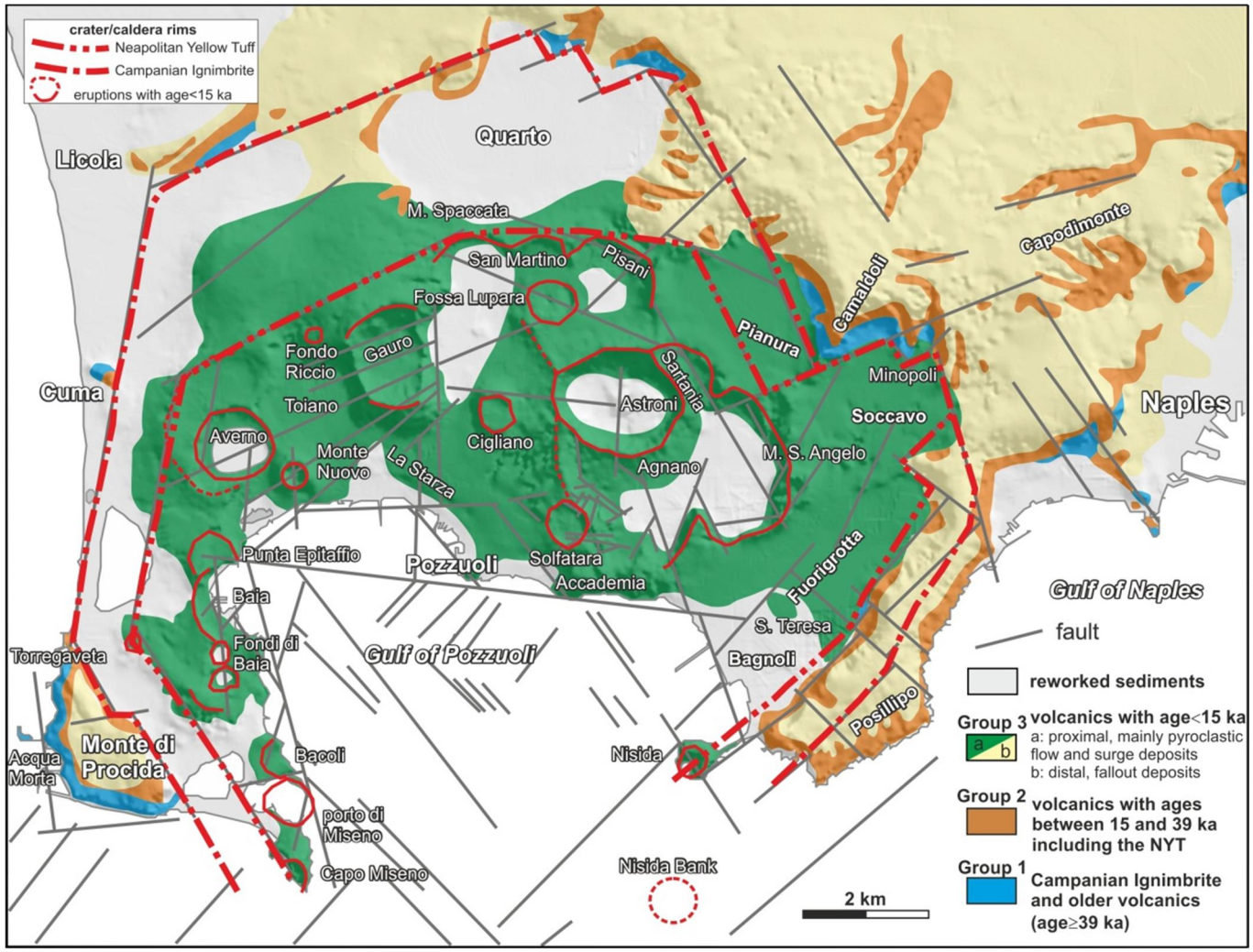

Fig 3. Simplified geological map of Campi Flegrei caldera showing regional fault traces and main morphological structures.

Outline

The described application includes two parts, dedicated to long term hazard assessments.

I. a map of probability for **the location** of the next eruptive vent
(see Bevilacqua et. al 2015)

II. a probability distribution for **the size** of the next pyroclastic density current (PDC), and a map of probability for the **PDC invasion hazard**
(see Neri et al. 2015)

Uncertainty quantification based on expert judgment, concerning size and location of the next PDC has strong implications on the hazard estimates.

Also the poster presentation Tadini et al. of this workshop, focuses on the Somma-Vesuvio vent opening map development through a similar approach.

Long-term temporal assessments are not included in this presentation, and the estimates are always **conditional on the next event** occurrence.

A doubly stochastic model for the episodic volcanism of Campi Flegrei is developed in Bevilacqua 2016.

PART I

Vent opening probability maps

A key aspect of the study was the **identification**, and where possible the **quantification**, of some of the main **sources of epistemic uncertainty** that are associated with the available data.

- the **uncertainty on location** of past eruptive vents;
- the number of past events which do not correspond to presently identified locations ('**lost vents**');
- the **uncertainty of linear weights** of different probability measures contributing to the vent opening map definition.

The physical variability is assessed with a **linear combination** of 7 spatial distributions $(\mu_i)_{i=1,\dots,d}$ of key variables of the system that reflect, or can influence, this volcanic process.

Vents Epoch I	*Vents Epoch II*	*Vents Epoch III*	*Lost vents*	*Faults*	*Fractures*	*Homog. map*

It was included a uniform probability measure, **homogeneous** over the NYT caldera, for representing the possible lack of information. Lost vents have been assumed uniformly on the **inland** portion of the caldera.

The assessment of the vent opening map $\sum_{i=1}^{d} \alpha_i(e)\mu_i$, is reduced to find the distribution of the positive random coefficients $\alpha = (\alpha_i)_{i=1,\dots,d}$, $\sum_i^d \alpha_i = 1$ depending on the epistemic uncertainty *e*.

The first three probability maps are obtained from the renormalized sum of **uniform probability distributions** inside ellipses enclosing the **uncertain/enlarged locations** of past vents/fissures during each epoch of activity.

Large ellipses mostly indicate lack of constraints and **large uncertainty** in the locality of the vent.

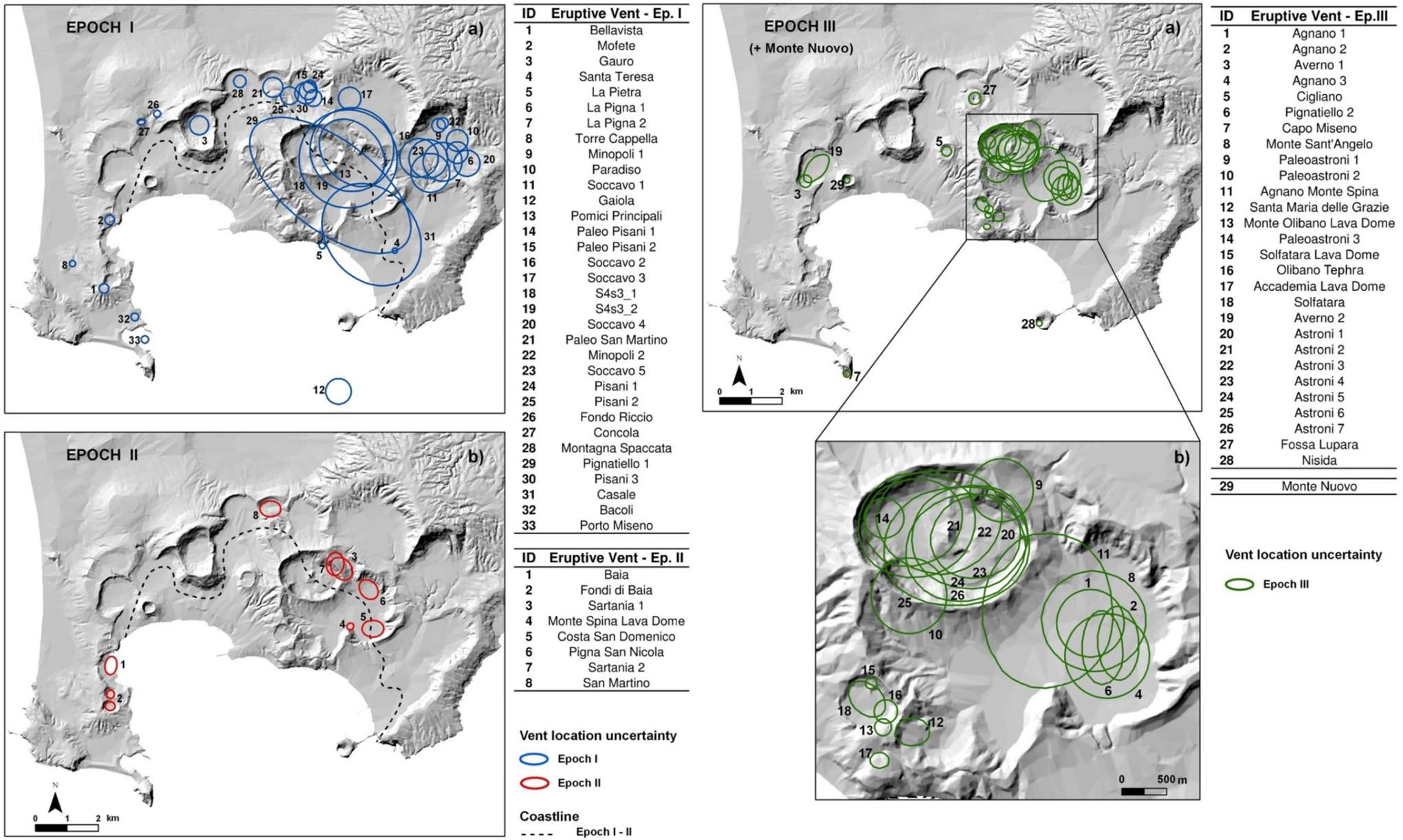

ID	Eruptive Vent - Ep. I
1	Bellavista
2	Mofete
3	Gauro
4	Santa Teresa
5	La Pietra
6	La Pigna 1
7	La Pigna 2
8	Torre Cappella
9	Minopoli 1
10	Paradiso
11	Soccavo 1
12	Gaiola
13	Pomici Principali
14	Paleo Pisani 1
15	Paleo Pisani 2
16	Soccavo 2
17	Soccavo 3
18	S4s3_1
19	S4s3_2
20	Soccavo 4
21	Paleo San Martino
22	Minopoli 2
23	Soccavo 5
24	Pisani 1
25	Pisani 2
26	Fondo Riccio
27	Concola
28	Montagna Spaccata
29	Pignatiello 1
30	Pisani 3
31	Casale
32	Bacoli
33	Porto Miseno

ID	Eruptive Vent - Ep. II
1	Baia
2	Fondi di Baia
3	Sartania 1
4	Monte Spina Lava Dome
5	Costa San Domenico
6	Pigna San Nicola
7	Sartania 2
8	San Martino

ID	Eruptive Vent - Ep.III
1	Agnano 1
2	Agnano 2
3	Averno 1
4	Agnano 3
5	Cigliano
6	Pignatiello 2
7	Capo Miseno
8	Monte Sant'Angelo
9	Paleoastroni 1
10	Paleoastroni 2
11	Agnano Monte Spina
12	Santa Maria delle Grazie
13	Monte Olibano Lava Dome
14	Paleoastroni 3
15	Solfatara Lava Dome
16	Olibano Tephra
17	Accademia Lava Dome
18	Solfatara
19	Averno 2
20	Astroni 1
21	Astroni 2
22	Astroni 3
23	Astroni 4
24	Astroni 5
25	Astroni 6
26	Astroni 7
27	Fossa Lupara
28	Nisida
29	Monte Nuovo

Fig 7. Reconstruction of the location of the eruptive vents and fissures for the events occurred in the three epochs of activity. The dashed line indicates the likely location of the coast line between Epochs II and III. Names of the events updated from Smith et al. 2011.

Based on experts opinion, we partitioned the caldera in 16 zones $(A_l)_{l=1,\dots,N}$ with different features and history of activity, separating the **spatial and temporal clusters** of past vents.
The first 13 zones have the same extent.

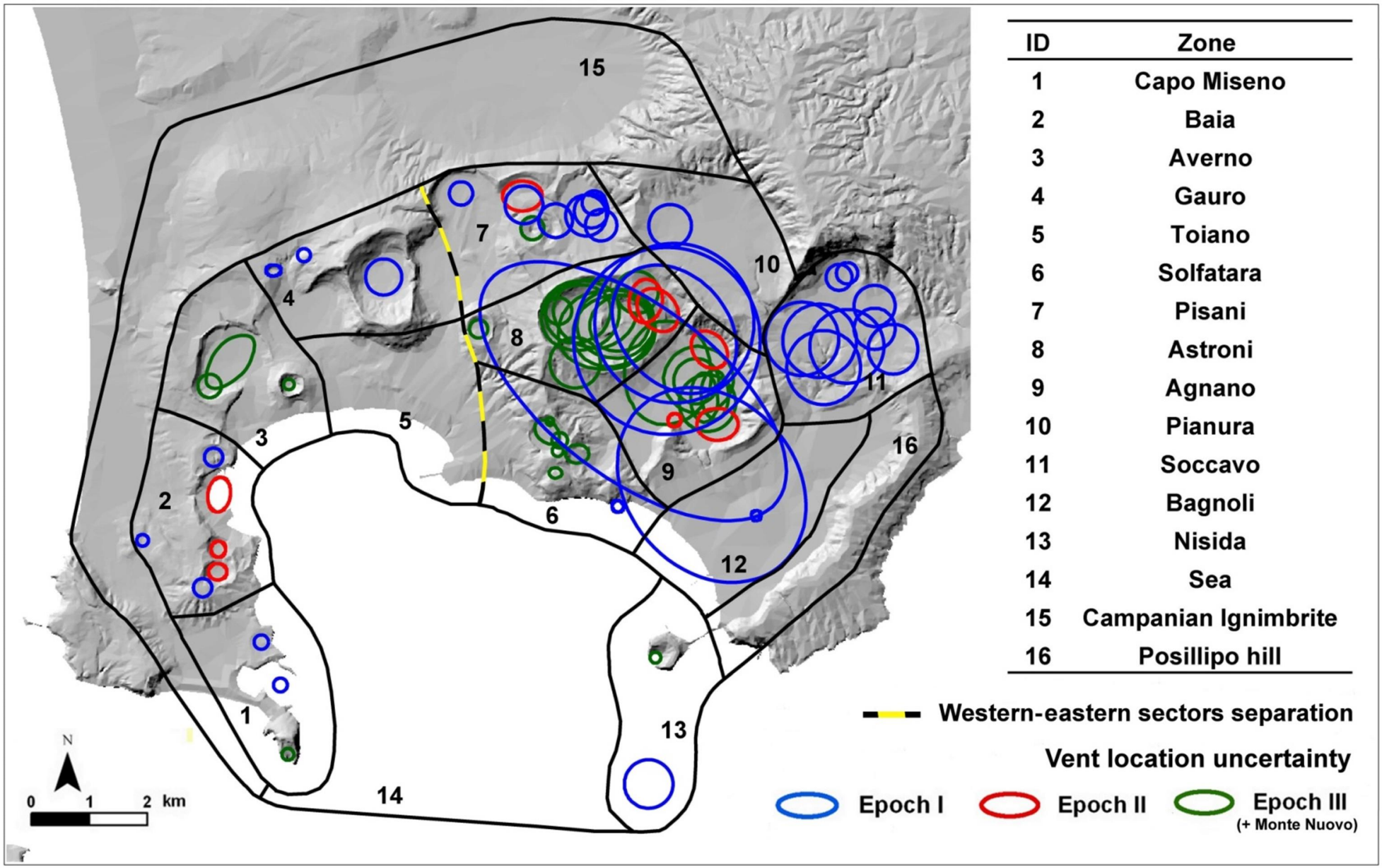

ID	Zone
1	Capo Miseno
2	Baia
3	Averno
4	Gauro
5	Toiano
6	Solfatara
7	Pisani
8	Astroni
9	Agnano
10	Pianura
11	Soccavo
12	Bagnoli
13	Nisida
14	Sea
15	Campanian Ignimbrite
16	Posillipo hill

Fig 8. Partitioning of the caldera in 16 zones. The colours of the ellipses correspond to the epoch of activity.
The yellow dashed line separates eastern and western sectors.

We convolved a two dimensional symmetric **Gaussian kernel** with the uniform probability measures enclosed in the uncertainty ellipses (e.g. Connor and Hill 1995; Mazzarini et al. 2003).
This produced a simplified **map of vent opening** based only on the past vents locations (Fig a).

We got consistent results which include more geological information, assuming uniform probability inside each **zone of the partition** in proportion with the number of ellipses contained (Fig b).
Separated maps have been produced for each epoch of activity, to combine them with different weights.

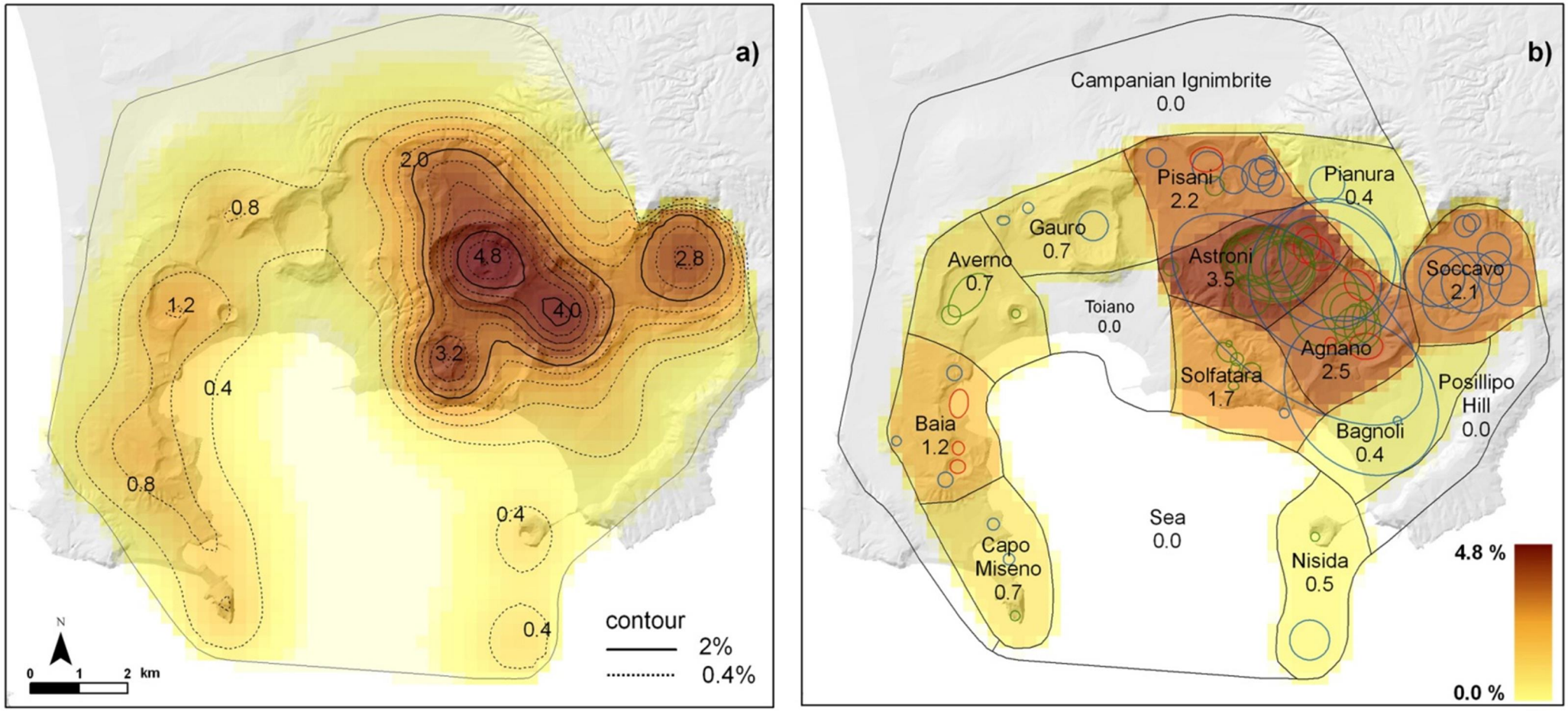

Fig 9. Density distribution of the probability of vent opening obtained using the past vent location data by: (a) kernel density estimation and (b) partitioning of the caldera in 16 homogeneous zones.
Values reported in the different subareas and on the contours indicate the percentage probability of vent opening per km^2.

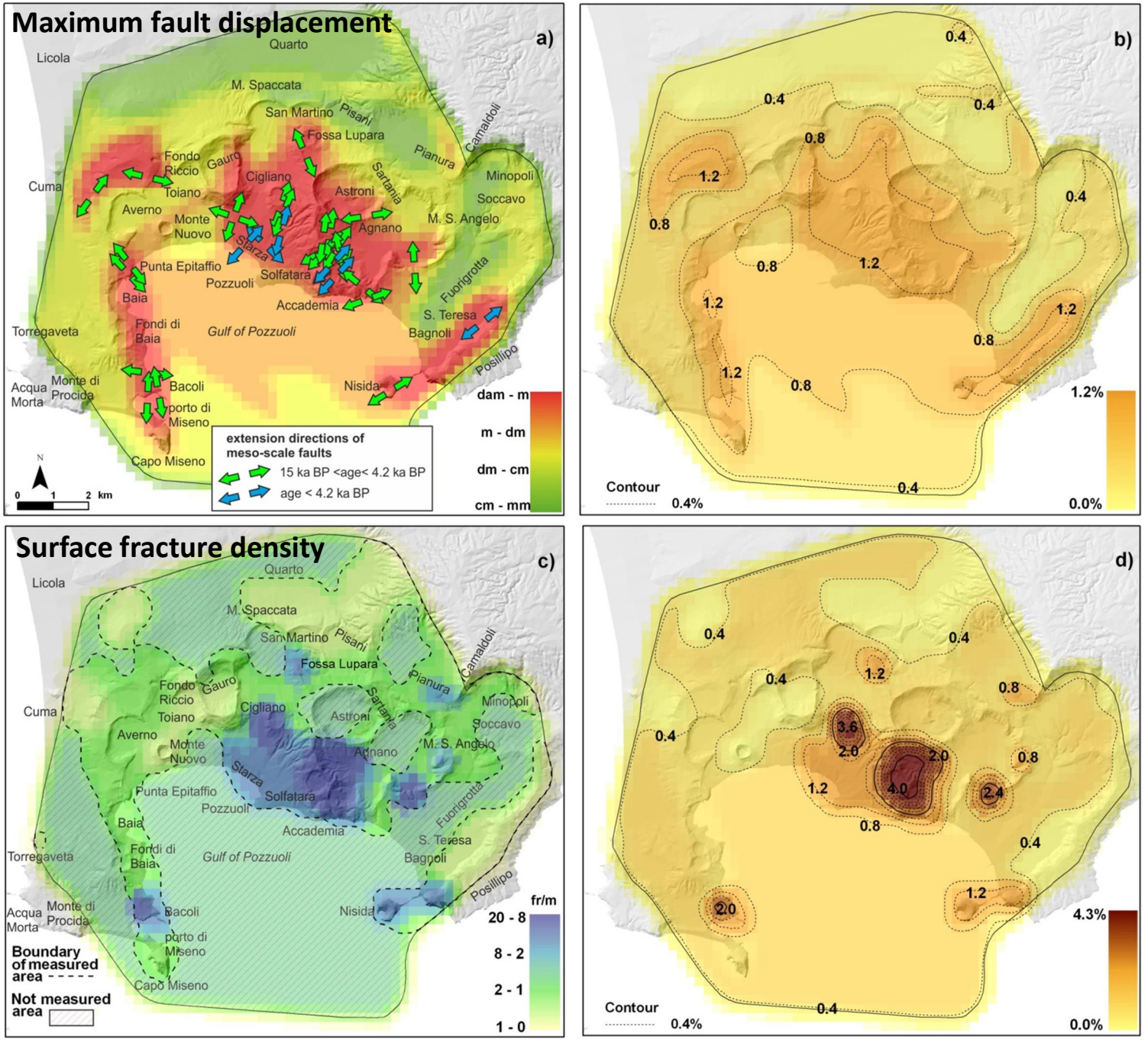

Other probability maps concern the structural features.
(e.g. Vitale and Isaia 2014)

The **faults map** shows the value of density of fault displacement taking into account the historical deformation patterns.

The **fractures map** shows the value of density of fracturation, as number of fractures per meter, obtained from discrete sampling.

Fig 10. (a) Maximum fault displacement in the caldera, with extensional directions. The colour levels correspond to different orders of magnitude. (c) Surface fracture density in the caldera. Values of density range between about 1 and 20 fr/m. Wide areas were not measured (dashed areas), and the average value of the measured zone was assumed. (b-d) Density distributions of the probability of vent opening obtained normalizing the values.

The **structured and performance based elicitation sessions** were performed to make more robust the choice of the weights of the maps.

Several elicitation sessions, involving **8 experts** with different volcanological backgrounds were carried out through **meetings** and also email consultations.

The **seed questions** were about particular aspects of Campi Flegrei volcanism, other Italian volcanoes, and about explosive volcanism in general.

To simplify the quantification of the weights of each spatial distribution to combine, the **target questions** did not ask for them directly: a **simple hierarchical logic tree** was defined instead.

Most of the target questions quantified the **relative importance**, or relevance, of one variable or feature of the system versus others.

Other relevant questions were about the estimation of the **number of 'lost vents'** in each epoch of activity.

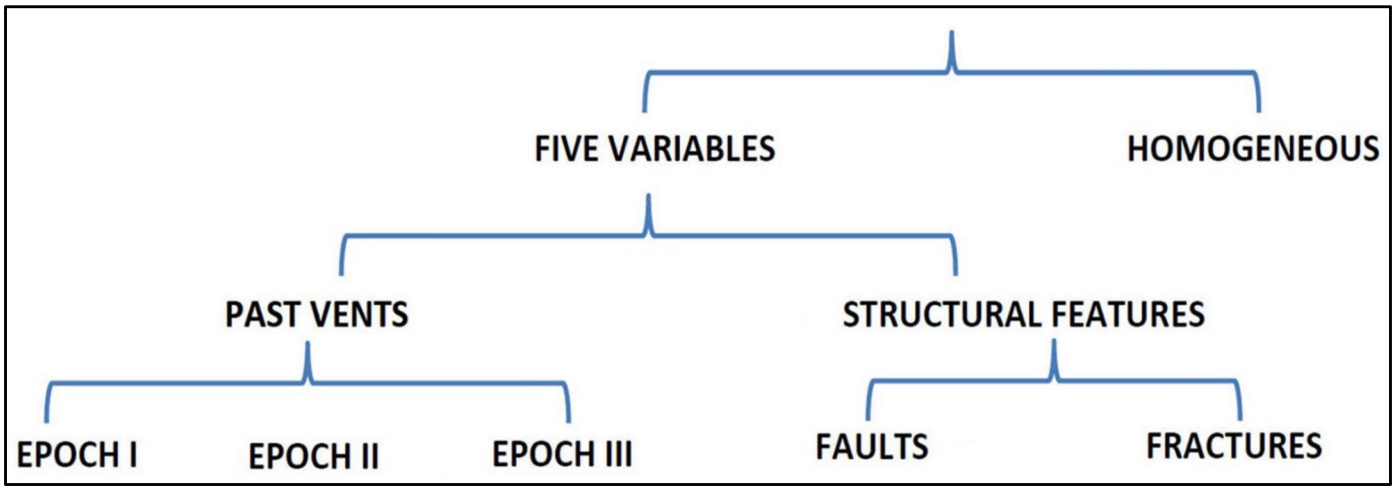

Fig 14. Hierarchical logic tree structure associated to the target questions queried during the elicitation sessions.

We followed a **Monte Carlo simulation approach**, multiplying the single estimates over each branch of the logic tree to obtain the probability distributions of the weights.

Tab 2. Probability percentages of the mean and 5*th* and 95*th* percentiles of the weights with respect to the CM, ERF and EW methods.

Variable/ Method	*Vents Epoch I*	*Vents Epoch II*	*Vents Epoch III*	*Lost vents*	*Faults*	*Fractures*	*Homog. map*	**Statistics**
CM	*6.3*	*1.3*	*10.2*	*3.3*	*8.1*	*5.4*	*6.3*	*5%ile*
	16	***4.5***	***20.4***	***5.9***	***16.4***	***11.9***	***24.9***	***Mean***
	26.7	*8.7*	*33.3*	*9*	*26.6*	*20.4*	*42.4*	*95%ile*
ERF	*9.5*	*2.2*	*14.7*	*4.2*	*10.2*	*7*	*8.7*	*5%ile*
	16.4	***4.8***	***22.5***	***6.3***	***16.5***	***12.3***	***21.3***	***Mean***
	24	*7.6*	*31.6*	*8.8*	*23.9*	*18.6*	*31.1*	*95%ile*
EW	*6.3*	*1.5*	*7.6*	*3.4*	*5.3*	*4.3*	*6.5*	*5%ile*
	17.7	***4.6***	***19.3***	***6.7***	***13.8***	***12***	***25.9***	***Mean***
	30.5	*9.3*	*33.8*	*11*	*24.3*	*22*	*45.4*	*95%ile*

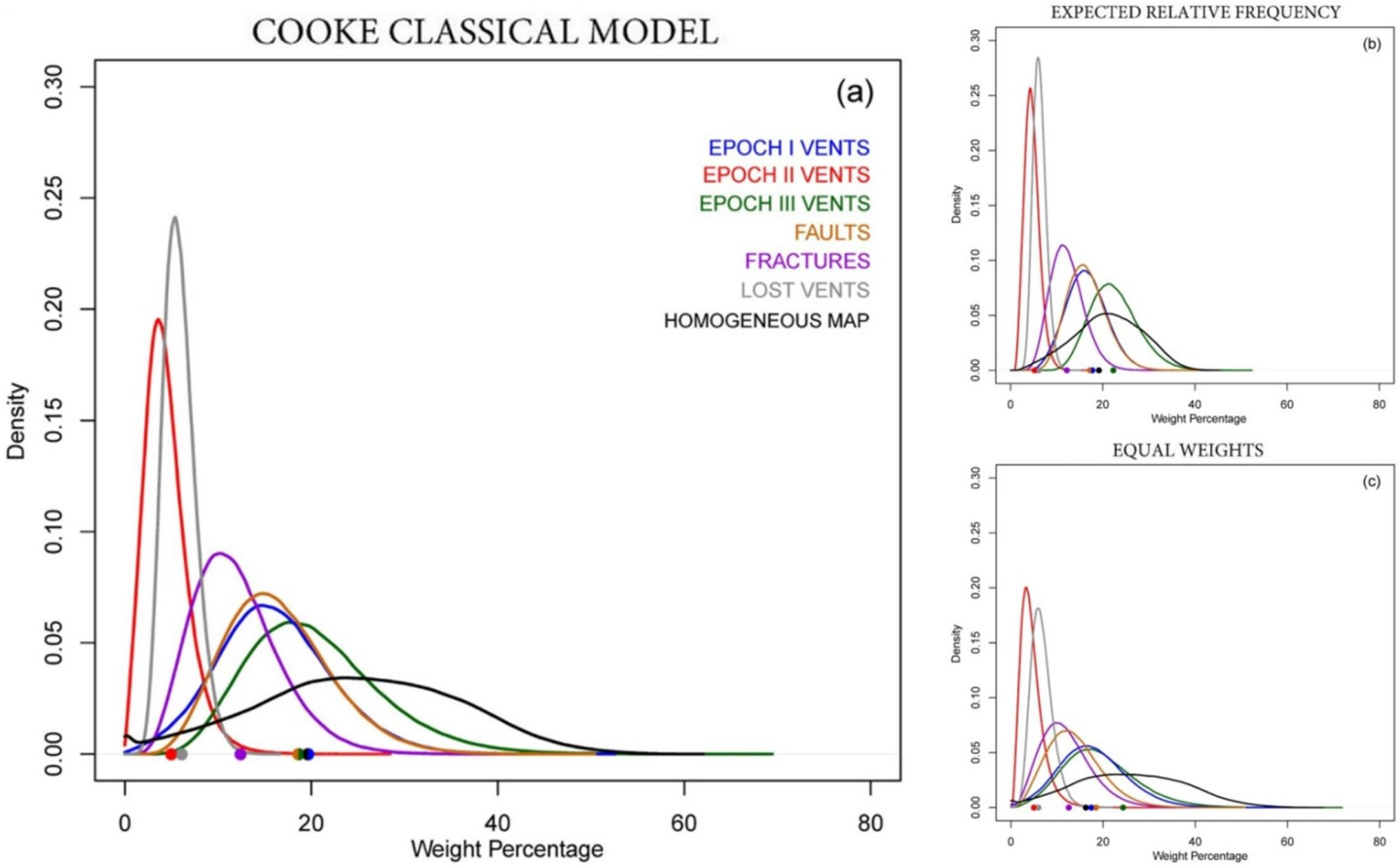

Fig 15. Pdfs of the weights from the elicitation models assumed, i.e., (a) Cooke CM, (b) ERF model, and (c) EW model.

Along the x axis are also reported as coloured dots the estimates obtained by using just the best guess (central) values of the experts.

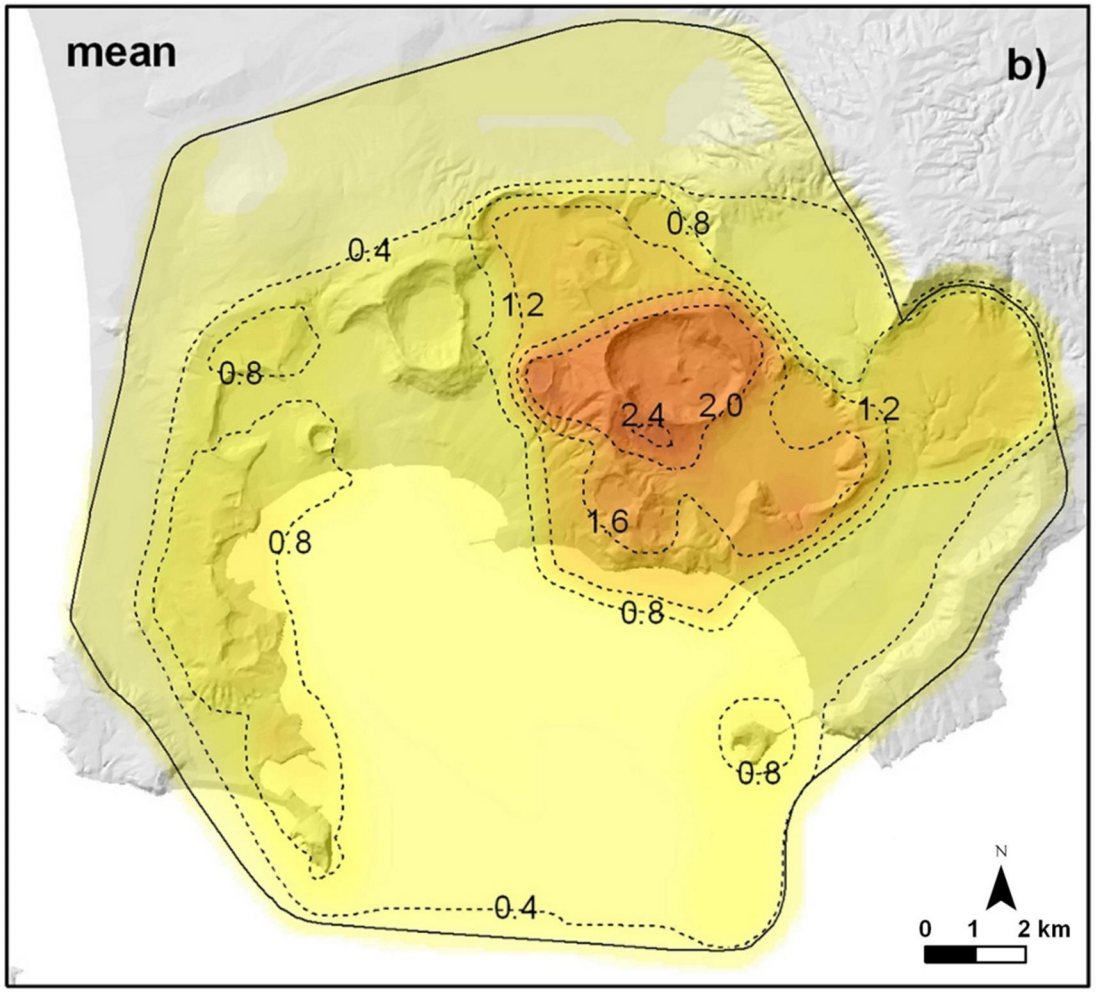

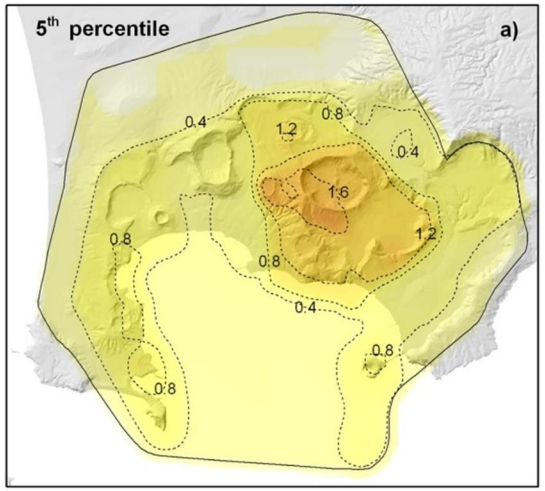

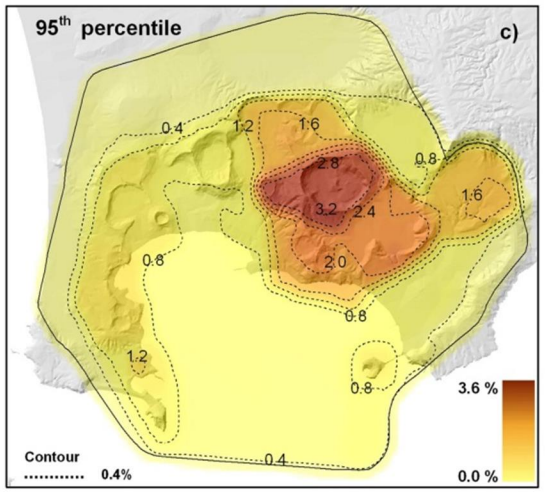

Fig 16. Probability density maps of new vent opening location.

(a), (b) and (c) refer to the 5*th* percentile, mean and 95*th* percentile values of the density, with respect to epistemic uncertainty.

Contours and colours indicate the percentage probability of vent opening per km^2 conditional on the occurrence of an eruption.

Results have shown evidence for a main **high probability** region in the **central-eastern portion of the caldera**. Significantly lower **secondary largest** are found to exist in both the **eastern and western parts of the caldera**.

Nevertheless the spatial distribution of vent opening position **probability is widely dispersed** over the whole NYT caldera, including the offshore portion.

We accompany the probabilities with **quantified uncertainty estimates** which are indicative, typically, of spreads ±30% on the local mean value.

PART II

Pyroclastic density current invasion hazard maps

In our analysis, we designated the **areas invaded (inundated) by the past PDCs** as a variable representative of the distribution of the next PDC magnitudo. We focused on the more dilute part of the flows (surge-like).

ID	PDC Deposit - Epoch I	Area (km^2)
1	Bellavista Volcano	3.9
2	Mofete Volcano	2.1
3	Gauro Volcano	16.1
4	Santa Teresa Volcano	0.9
5	La Pietra Volcano	2.6
8	Torre Cappella Volcano	1.0
11	Soccavo 1 Tephra	190.5
13	Pomici Principali Tephra	129.2
14	Paleo Pisani 2 Tephra	37.7
16	Soccavo 2 Tephra	75.8
17	Soccavo 3 Tephra	147.5
20	Soccavo 4 Tephra	180.2
21	Paleo San Martino Tephra	37.3
22	Minopoli 2 Tephra	113.6
23	Soccavo 5 Tephra	66.2
25	Pisani 2 Tephra	21.1
28	Montagna Spaccata Tephra	3.0
30	Pisani 3 Tephra	3.0
32	Bacoli Volcano	1.1
33	Porto Miseno Volcano	0.7

ID	PDC Deposit - Epoch II	Area (km^2)
2	Fondi di Baia Tephra	15.7
3	Sartania 1 Tephra	40.7
5	Costa San Domenico Tephra	16.9
6	Pigna San Nicola Tephra	8.0
7	Sartania 2 Tephra	27.0
8	San Martino Tephra	19.7

ID	PDC Deposit - Epoch III	Area (km^2)
2	Agnano 2 Tephra	17.1
3	Averno 1 Tephra	27.0
4	Agnano 3 Tephra	68.0
5	Cigliano Tephra	28.3
7	Capo Miseno Volcano	1.1
8	Monte Sant'Angelo Tephra	43.8
9	Paleoastroni 1 Tephra	18.1
10	Paleoastroni 2 Tephra	5.4
11	Agnano Monte Spina Tephra	312.5
18	Solfatara Tephra	8.7
19	Averno 2 Tephra	24.8
20	Astroni 1 Tephra	39.7
21	Astroni 2 Tephra	19.1
22	Astroni 3 Tephra	41.1
23	Astroni 4 Tephra	60.4
24	Astroni 5 Tephra	29.1
25	Astroni 6 Tephra	26.9
26	Astroni 7 Tephra	10.2
27	Fossa Lupara Tephra	8.9
28	Nisida Tephra	4.7
29	Monte Nuovo Tephra	5.7

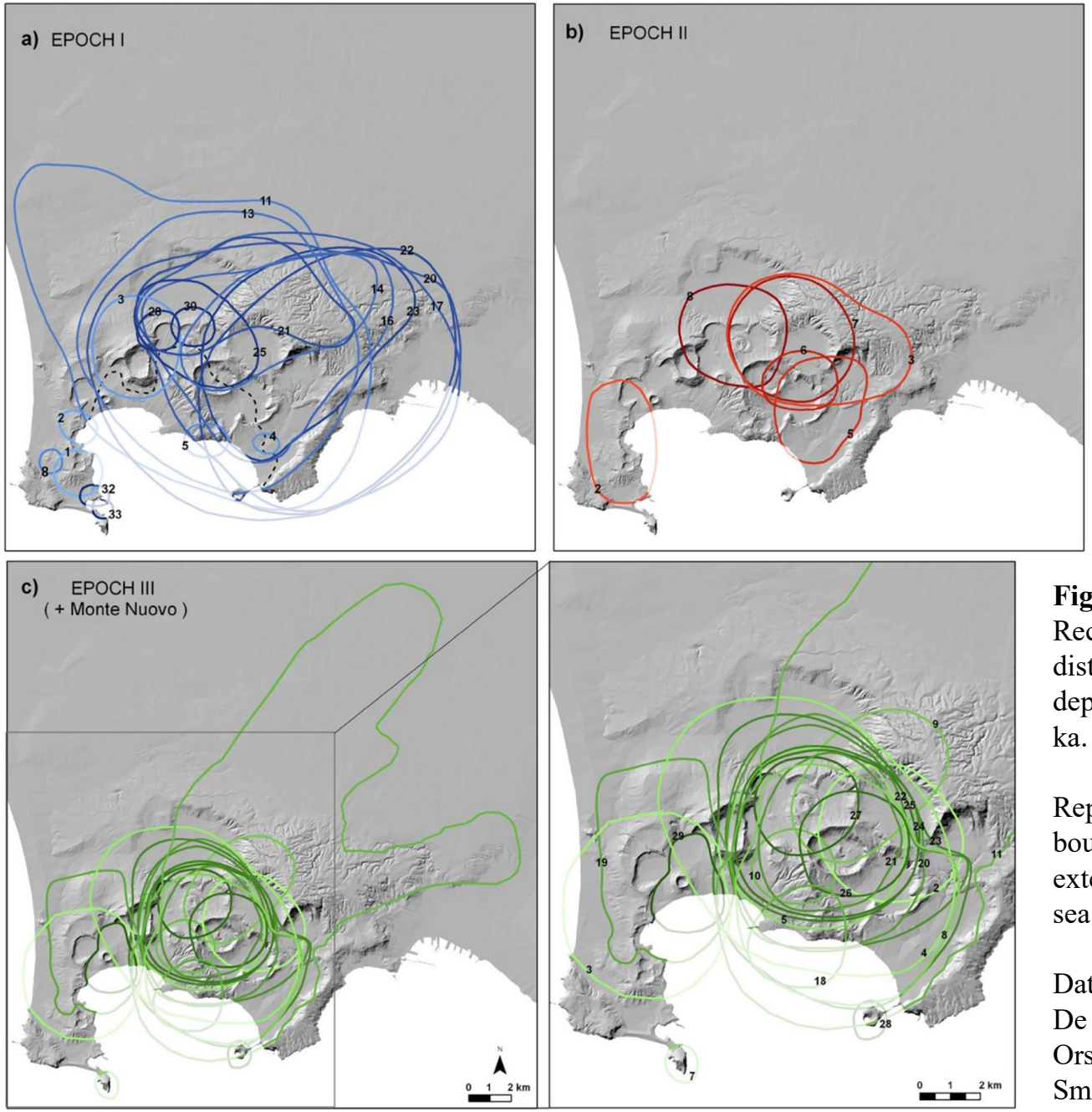

Fig 17.
Reconstruction of the distribution of PDC deposits of the last 15 ka.

Reported deposit boundaries were extended over the sea.

Data modified from De Vita et al. 1999; Orsi et al. 2004; Smith et al. 2011.

Again the **identification**, and where possible the **quantification**, of some of the main **sources of epistemic uncertainty** is a key aspect.

In this case:

• the **radial underestimation error** of deposit boundaries (elicited between 150m and 1000m);

• the **lost PDCs** invasion areas (randomly extracted following the known invasion areas);

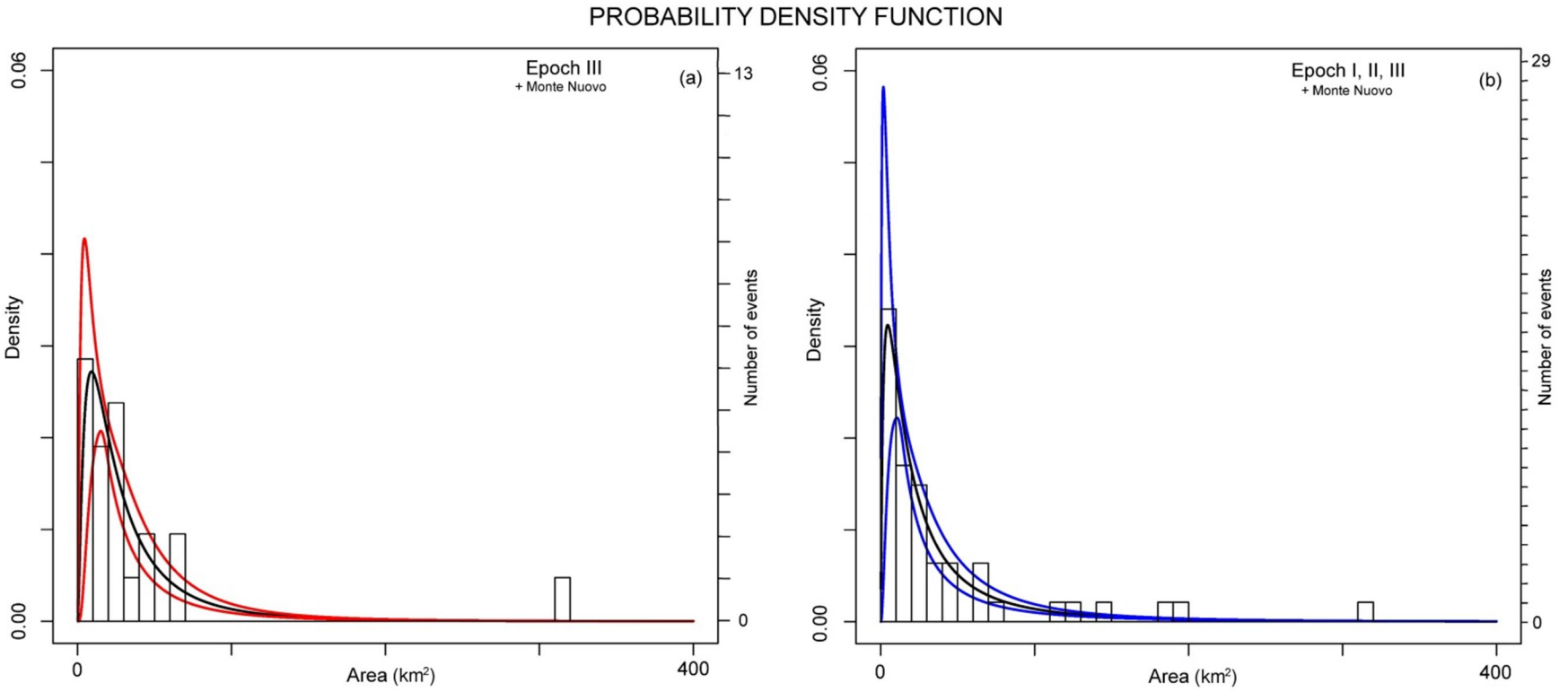

Figure 18. Histograms of the PDC invasion areas and probability density functions for the invasion areas.

The black curve is the mean and the coloured curves are the 5*th* and 95*th* uncertainty percentiles

We adopted a maximum likelihood lognormal distribution, but also Power law or Weibull were considered.

We based the hazard assessment on the construction of a set function *F* such that *F(x,y)* represents the set invaded by a PDC propagating from a vent located in *x* with an area extension *y*.

The dynamics of the PDC is described as the **collapse of a constant volume of dense fluid** in a lighter one and on a flat surface (e.g. Huppert and Simpson 1980; Dade and Huppert 1996; Harris et al. 2002).

Dynamical system of the front position 'Box Model'

$$\begin{cases} u = \dfrac{dl}{dt} = Fr(g_p \phi h)^{1/2}, & \text{(Von Kàrman, 1940)} \\ \dfrac{d\phi}{dt} = -w_s \dfrac{\phi}{h}, & \text{(Particles deposition)} \\ l^2 h = V. & \text{(Geometric condition) (axisymmetric)} \end{cases}$$

$$g_p = \frac{\rho_p - \rho_a}{\rho_a} g \quad \text{(Reduced gravity)}$$

Different geometric constrains, i.e. rectangular, lead to different solution.

We calculated the **relationship between front position and time** as a function of initial conditions.

$$l(t) = [\tanh(t/\tau)]^{1/2} \, l_{max}$$

$$\tau = \left(Fr^{-1}(g_p \phi_0 V)^{-1/2} l_{max}^2\right)/2$$

$$l_{max} = \left(8\phi_0^{1/2} g_p^{1/2} V^{3/2} w_s^{-1} Fr\right)^{1/4}$$

w_s is the settling velocity of the particles
ϕ_0 is the initial volume fraction of the particles
V is the constant volume (divided by π)

Fr is the Froude number, representing the relation between inertial and gravitational forces.

It is possible to calculate a function *K* such that $K(r, l_{max})$ is the kinetic energy of a PDC with maximum run-out l_{max} at a distance *r* from the vent.

$$K(r, l_{max}) = \frac{1}{2}\left[\frac{C l_{max}^{1/3}}{\hat{r}\cosh^2 artanh(\hat{r}^2)}\right]^2$$

$$\hat{r} = r/l_{max}$$

$$C = \left(Fr^2 w_s \phi_0 g_p\right)^{1/3}/2$$

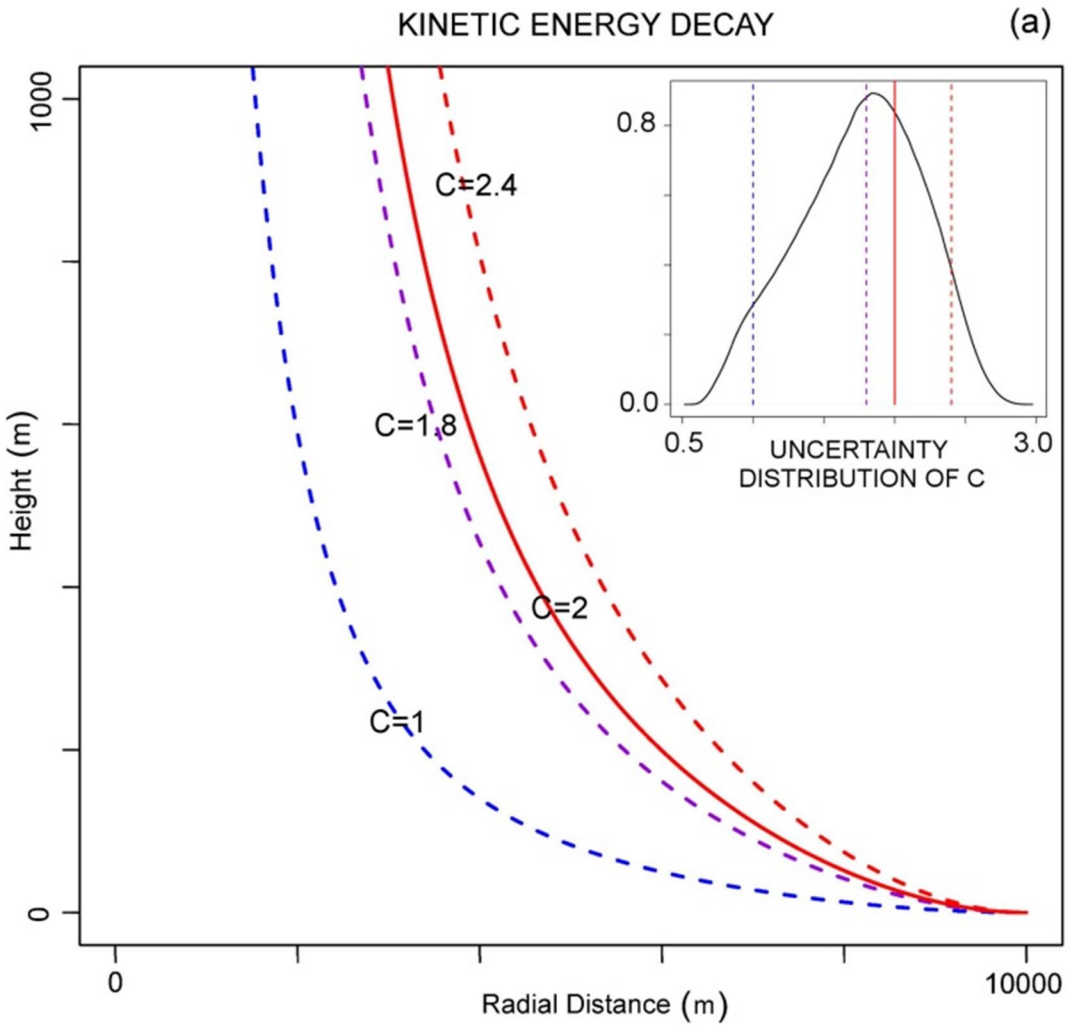

We compared the **kinetic energy** of the flow front with the height of the **topographic relief** potentially reached/overcome, finding the set of the points which the current has **enough energy** to reach.

This PDC invasion model was applied in an **inverse mode,** repeated for each sample of a Monte Carlo simulation varying vent location and PDC areal size.

Fig 19. (a) Example of decay of radial flow head kinetic energy as a function of distance from the source. An example of a probability density function for the C parameter is shown.

Curves refer to a flow run-out of 10 km and to values of the C.

The PDC invasion hazard maps with uncertainty

The mean and percentile **PDC invasion hazard values** with respect to the epistemic uncertainty, were mapped in each point of the Campi Flegrei area.

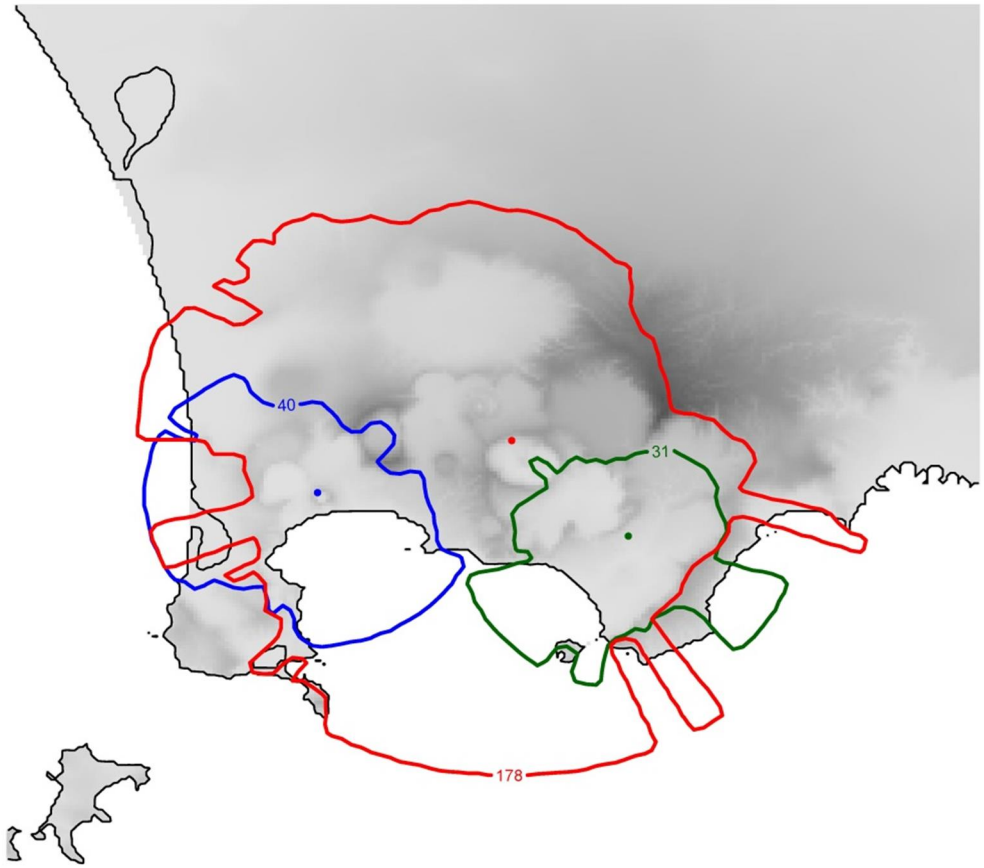

We combined:
- the spatial probability **map of new vent opening**,
- the probability distribution of **PDC invasion areas,**
- by using the **simplified propagation model.**

The inverse mode adopted strongly linked the PDC hazard estimates to the past deposits extents but required to numerically **invert the propagation model** during each simulation.

Fig 20. Examples of single PDC propagations, assuming different vent locations (the colored points) and areal sizes in km^2 (the numbers reported on the curves).

All our maps relate solely to the **probability of invasion** by PDCs and not to the distributions of specific hazard variables.

It was assumed that a future PDC episode will originate in the **onland portion** of the caldera because source conditions would be fundamentally and significantly different in the case of an underwater vent.

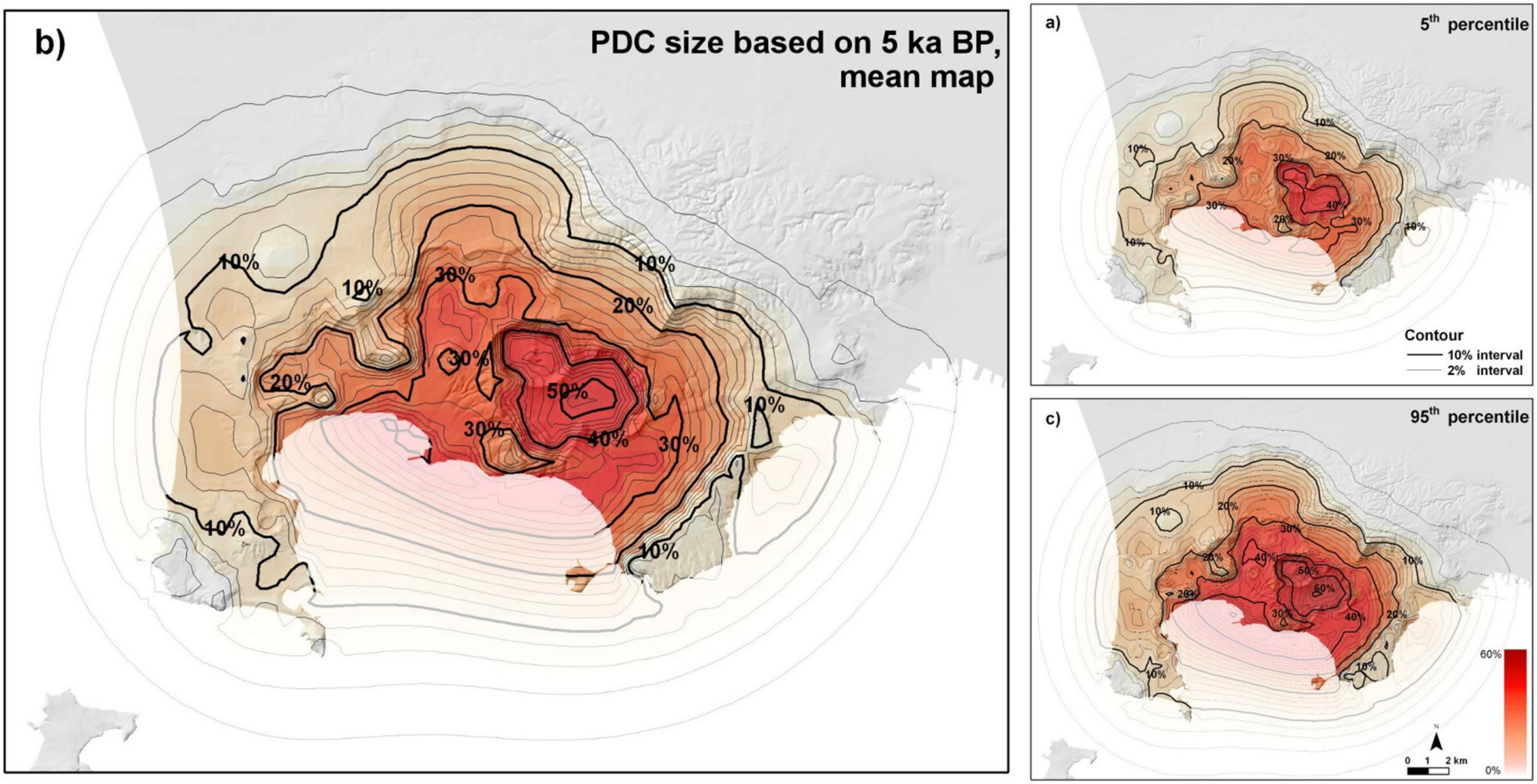

Fig 21. PDC invasion probability maps based on invasion areas of the last 5 ka, a single vent per eruption, located in the on-land part of the caldera. Contours and colours indicate the percentage probability of PDC invasion conditional on the occurrence of an explosive eruption.

Mean invasion probabilities above 5% are calculated over the **whole CI caldera**, with peak values exceeding 50% in the Agnano plain.

Mean probabilities above 10% are also computed in some areas **outside** the caldera, across Posillipo hill.

Uncertainty ranges affecting invasion probabilities inside the caldera lay between ±15 and ±35% of the local mean value; wider uncertainties are found outside the caldera, with an average above ±50%.

Concluding remarks

- Performance-based **expert judgment techniques** are promising methods for providing uncertainty quantification when more accurate models are not available, for example when the sources of epistemic uncertainty are significant.

- **Doubly stochastic models** are a very general tool for assessing random systems that depend on uncertain information, as in the case of volcanic processes.

- The '**logic tree**' approach is an easy method for combining alternative vent opening maps based on key volcanologic features, inside a doubly stochastic model.

- A PDC invasion area estimation based on **continuous probability** density functions extends the classical hazard approach relying on separate scenarios for specific eruption sizes and are a simple approach to produce comprehensive hazard assessments.

- The next development of this study is the convolution of the produced hazard maps conditional on the occurrence of an eruption, with **long-term time assessments** able to describe the episodic volcanism at Campi Flegrei.

Publications

Quantifying volcanic hazard at Campi Flegrei caldera (Italy) with uncertainty assessment: I. Vent opening maps, *A. Bevilacqua , R. Isaia, A. Neri, S. Vitale , W. P. Aspinall, M. Bisson, F. Flandoli, P. J. Baxter, A. Bertagnini, T. Esposti Ongaro, E. Iannuzzi, S. Orsucci, M. Pistolesi, M. Rosi,* J Geophys Res, 120 (4), 2309-2329.

Quantifying volcanic hazard at Campi Flegrei caldera (Italy) with uncertainty assessment: II. Pyroclastic density current invasion maps, *A. Neri, A. Bevilacqua, T. Esposti Ongaro, R. Isaia, W. P. Aspinall, M. Bisson, F. Flandoli, P. J. Baxter, A. Bertagnini, E. Iannuzzi, S. Orsucci, M. Pistolesi, M. Rosi, S. Vitale*, J Geophys Res, 120 (4), 2330-2349.

Doubly Stochastic Models for Volcanic Hazard Assessment at Campi Flegrei Caldera, *A. Bevilacqua*, "PhD Thesis", Edizioni della Normale, Birkhäuser/Springer, (accepted).

Acknowlegments

The obtained results were made achievable thanks to the precious collaboration with many colleagues in the ambience of several research projects, including:

- **Project MED-SUV** "*Mediterranean Supersite Volcanoes*", European Union, 2013-2016.
- **Project DPC-V1** "*Valutazione della pericolosità vulcanica in termini probabilistici*", Dipartimento della Protezione Civile (Italy), 2012-2015.
- **Project EJN** "*Expert Judgment Network*", COST Action, European Union, 2013-2017.

SCUOLA NORMALE SUPERIORE

INGV

SEVENTH FRAMEWORK PROGRAMME

MEDiterranean SUpersite Volcanoes MED-SUV

PROTEZIONE CIVILE NAZIONALE

Unione Europea

cost EUROPEAN COOPERATION IN SCIENCE AND TECHNOLOGY